



Original Paper

Research on casing deformation prevention technology based on cementing slurry system optimization

Yan Yan ^{a, b, c}, Meng Cai ^d, Wen-Hai Ma ^d, Xiao-Chuan Zhang ^d, Li-Hong Han ^{a, *}, Yong-Hong Liu ^b

^a State Key Laboratory for Performance and Structure Safety of Petroleum Tubular Goods and Equipment Materials, CNPC Tubular Goods Research Institute, Xi'an, 710077, Shaanxi, China

^b College of Mechanical and Electrical Engineering, China University of Petroleum (East China), Qingdao, 266580, Shandong, China

^c Shale Gas Evaluation and Exploitation Key Laboratory of Sichuan Province, Chengdu, 610095, Sichuan, China

^d CNPC Daqing Oilfield Company, Daqing, 163453, Heilongjiang, China



ARTICLE INFO

Article history:

Received 2 March 2023

Received in revised form

18 October 2023

Accepted 19 October 2023

Available online 21 October 2023

Edited by Jia-Jia Fei

Keywords:

Cement slurry

Hollow ceramicsite

Casing deformation

Formation slip

Field test

ABSTRACT

The casing deformation prevention technology based on the optimization of cement slurry is proposed to reduce the casing deformation of shale oil and gas wells during hydraulic fracturing. In this paper, the fracture mechanism of hollow particles in cement sheath was firstly analyzed by discrete element method, and the effect of hollow particles in cement on casing deformation was investigated by laboratory experiment method. Finally, field test was carried out to verify the improvement effect of the casing deformation based on cement slurry modification. The results show that the formation displacement can be absorbed effectively by hollow particles inside the cement transferring the excessive deformation away from casing. The particles in the uncemented state provide deformation space during formation slipping. The casing with diameter of 139.7 mm could be passed through by bridge plug with the diameter of 99 mm when the mass ratio of particle/cement reaches 1:4. According to the field test feedback, the method based on optimization of cement slurry can effectively reduce the risk of casing deformation, and the recommended range of hollow microbeads content in the cement slurry is between 15% and 25%.

© 2023 The Authors. Publishing services by Elsevier B.V. on behalf of KeAi Communications Co. Ltd. This is an open access article under the CC BY-NC-ND license (<http://creativecommons.org/licenses/by-nc-nd/4.0/>).

1. Introduction

Hydraulic fracturing has been widely used in shale oil/gas around the world. During fracturing, casing diameter need be maintained large enough to ensure tools passing through the wellbore (Lian et al., 2015; Yu et al., 2016, 2022). Casing deformation in the horizontal section severely restricts fracturing operations, resulting in fracturing failure and lower oil/gas recovery. Scholars have carried out a lot of studies on the casing deformation analysis (Yan et al., 2017; Yin et al., 2018a; Li H.T. et al., 2020; Zhang et al., 2020a, b; Li et al., 2021a). It is generally approved that the formation slip and local high pressure are main reasons for casing deformation. Especially, natural fractures or artificial fracture network will lead to uneven stress distribution near the wellbore,

and the casing-cement will be sheared or extruded by formation slip, which cause casing deformation and even damage (Xi et al., 2018, 2020; Liu et al., 2019b; Meng et al., 2020), resulting in economic losses (Furui et al., 2012; Peng et al., 2007; Guo et al., 2020). Therefore, it is significant to investigate the influence of formation slip on wellbore deformation and recommend the appropriate prevention measures for casing deformation.

A lot of research has been carried out about the optimization of cement slurry, but most of them focus on the mechanical performance to improve the cement integrity such as strength, elastoplasticity and so on (Wei et al., 2022; Cheng et al., 2023). Guo et al. (2020) and Teodoriu (2019) respectively developed composite cement suitable for high temperature environment in geothermal wells, and verified its mechanical properties through a series of experiments. Hudson et al. (2017), Santos et al. (2021), Jafariefad et al. (2017a, b) developed ductile cement slurry with different formulations to improve the cementing strength of interface and enhance their deformability. Adjei et al. (2021) proposed to use

* Corresponding author.

E-mail address: hanlihong@cnpc.com.cn (L.-H. Han).

bentonite instead of fly ash to develop a new weighted cement and tested its performance. The results showed that this slurry shortened the thickening time and improved cement compressive strength. In addition, Jafariefad et al. (2020) summarized the challenges encountered in the cementing process after the addition of nano-scale additives in cement, including expansion nano-scale additives for shrinkage reduction, nano-rubber/flexible particles for modification, and charged nano-particles for cement hardening. The role of nano-material additives is to enhance the sealing and durability of cement (Salehi et al., 2018; Quercia et al., 2016). To sum up, there are many researches on cement additives, but their aim is to improve the cementing interface bonding quality and lower its own damage. The addition of the above additives can only improve the mechanical properties of cement itself, but they will not provide additional protection for casing under the condition of formation slip (Fig. 1).

Geology slip has been treated as the main cause of casing deformation (Xi et al., 2019; Yin et al., 2018b; Dong et al., 2019; Li et al., 2021b). Xi et al. (2021) indicated the casing deformation prevention could not only rely on casing steel grade and thickness, but also optimizing the stage spacing, perforation density or temporarily block. Zhao et al. (2021) believed that casing deformation is caused by the geological migration during fracturing, so the propagation of geological fractures should be traced and measures should be taken such as enhancing cement strength and eliminating micro-annulus in wellbore. Liu et al. (2019a) investigated the influence of thickness and ovality of cement sheath on casing deformation. Guo et al. (2019) and Wang et al. (2021) considered that the casing deformation was comprehensively related to the non-uniform mechanics around the wellbore, poor cementing quality, and geological fractures. To sum up, the scholars have done a lot of theoretical analysis, however, the research on methods for controlling casing deformation is relatively few. Therefore, on the basis of hollowing cement, the effective casing deformation prevention method should be formed, which has reference value for preventing casing deformation under the condition of formation slip.

2. Discrete element model

2.1. Geometric model

According to the conventional well structure of shale gas in southwestern China, the outer diameter of production casing is 139.7 mm, the thickness of casing and cement sheath is 10.5 and 38.1 mm. The commercial software PFC^{2D} was used to establish the numerical model under extrusion condition. In order to improve

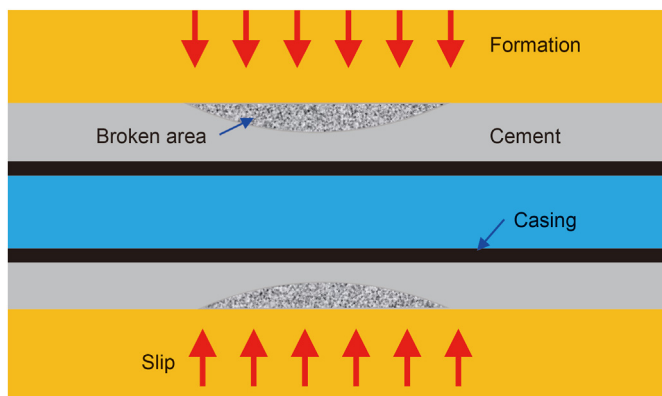


Fig. 1. Casing deformation mitigation by cement sheath.

the calculation speed, the cement length in the model is 20 mm. The size of the model is shown in Fig. 2. According to the logging data and previous research (Yang et al., 2023), the order of magnitudes is centimeter for shale slippage, thus the displacement boundary was set as 20 mm in this model. The end face of cement is the boundary of constant pressure and the subface of cement is fixed. Mechanical parameters should be defined in PFC^{2D} according to the actual physical parameters of cement and ceramite. The micro-mechanical parameters of these two materials are shown in Table 1.

2.2. Governing equation

Based on particle flow theory in PFC^{2D}, the parallel bonding model was used for contact between particles in order to get closer mechanical properties of cement particles and hollow particles.

The parallel bonding model provides the mechanical behavior of cement-based material between two contact slices (Li H. et al., 2020). The parallel bonded component interacts elastically between the slices. The parallel bonds does not exclude the possibility of slipping. They can transfer the forces and torques between the blocks and should be treated as a set of uniform elastic springs with constant normal and shear stiffness.

The contact force F_c and the contact torque M_c in parallel bonding model are:

$$F_c = F_1 + F_d + \bar{F} \quad (1)$$

$$M_c = \bar{M} \quad (2)$$

where F_1 is the linear force; F_d is the damping force; \bar{F} is the parallel bonding force; M is the parallel bonding torque.

The parallel bonding force can be decomposed into normal force and shear force, and the parallel bonding torque can be decomposed into torsional torque and bending torque:

$$\bar{F} = -\bar{F}_n \hat{n}_c + \bar{F}_s \quad (3)$$

$$\bar{M} = \bar{M}_b \quad (4)$$

where \bar{F}_n is the normal parallel bonding force; \bar{F} is the parallel bonding force; \hat{n}_c is unit normal vector in the contact surface; \bar{F}_s is shear force; \bar{M}_b is the bending torque.

The parallel bonding shear force \bar{F}_s and bonding torque \bar{M}_b are acted on the contact surface when the normal parallel bonding force $\bar{F}_n > 0$. They can be represented by the contact surface coordinate system:

$$\bar{F}_s = \bar{F}_{st} \hat{t}_c \quad (5)$$

$$\bar{M}_b = \bar{M}_{bs} \hat{s}_c \quad (6)$$

where \bar{F}_{st} is the parallel bonded shear stiffness; \bar{M}_{bs} is the parallel bonded bending stiffness; \hat{t}_c is the unit direction vector in the tension state; \hat{s}_c is the unit tangent vector of the contact surface.

An interface is set up between these two conceptual surfaces when a parallel bond is established and the parallel bond forces and torques are zeroed out. The parallel bond provides the elastic interaction between two conceptual surfaces, this interaction is invalid when the bonding is broken (Li H. et al., 2020). Each conceptual surface is rigidly attached to the component. The gap g_s of

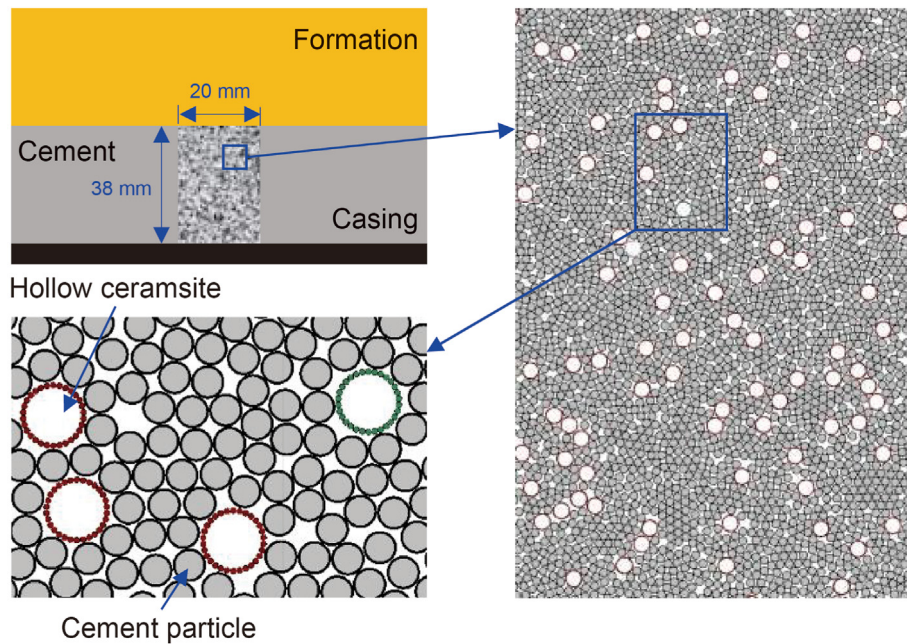


Fig. 2. Discrete element model of cement sheath with hollow particles.

Table 1
Microscopic parameters of cement and particle.

Material parameter	Cement	Hollow particle
Cement particle density ρ_s , $\text{kg}\cdot\text{m}^{-3}$	3150	1430
Radius of particle R_s , μm	50	100
Effective modulus with linear contact E_{mod} , GPa	0.5	0.81
Effective modulus of parallel bonding p_{b_emod} , GPa	0.5	0.81
Stiffness ratio k^*	1.0	1.0
Friction coefficient u	0.2	0.557
Tensile strength between particles p_{b_ten} , MPa	6	8.2
Cohesion between particles p_{b_coh} , MPa	26.7	6.56
Internal friction angle θ_{b_fa} , $^\circ$	17.797	30

the parallel bonding surface is defined as the cumulative relative normal displacement of the particle surface

$$\bar{g}_s = \sum_1^n \Delta\&n \tag{7}$$

where \bar{g}_s is the relative normal displacement increment of the contact between particles; It is indicated that the parallel bonding contact is not destroyed when $\bar{g}_s > 0$. Contact is divided into ball-to-ball contact and ball-to-surface contact, which is shown in Fig. 3.

2.3. Calculation results

Fig. 4 shows the particle geometry under the confining pressure of 30 MPa. As can be seen from Fig. 4, 8% high-strength hollow microbeads in cement has been broken before formation slippage due to the downhole hydrostatic pressure. The compressed hollow microbeads are squeezed circumferentially by the cement particles and the adjacent microbeads. The broken form of hollow microbeads is multi-segment strip. It is worth noting that tensile stress is distributed near the broken hollow beads caused by the compressed space. The high strength hollow microbeads randomly distributed in the solidified cement in the form of single broken particles and large pores composed of adjacent microbeads, as shown in Fig. 4. These pores will be collapsed firstly in the process

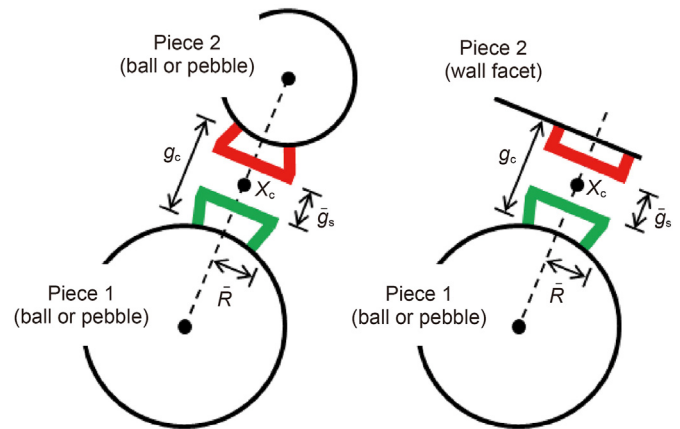


Fig. 3. Schematic diagram of parallel contact model.

of compression due to the lower strength.

A displacement loading of 20 mm was applied on the cement to simulate shale extrusion. The broken morphology under the slippage of 5, 10, 15 and 20 mm was shown in Fig. 5. All the hollow beads have been deformed when the formation slides down 5 mm, including the elastoplastic unbroken deformation, the broken uncompaction and the broken compaction. The unbroken hollow beads with elastoplastic deformation are usually elliptical or irregular. The broken hollow microbeads have lost their original supporting function, providing space for the formation slip. When the formation slides down from 5 to 10 mm, more hollow microbeads will be broken and further compacted. Because there are still a large number of unbroken microbeads in cement under the slippage of 5 mm. The characteristics of broken particles are shown in Fig. 5(c) when the formation slides down from 10 to 15 mm. The hollow beads are basically broken and compacted in this stage. It can be inferred that there is only compaction effect in cement sheath if the formation continues to slip downward. The cement with hollow beads is completely compacted when the

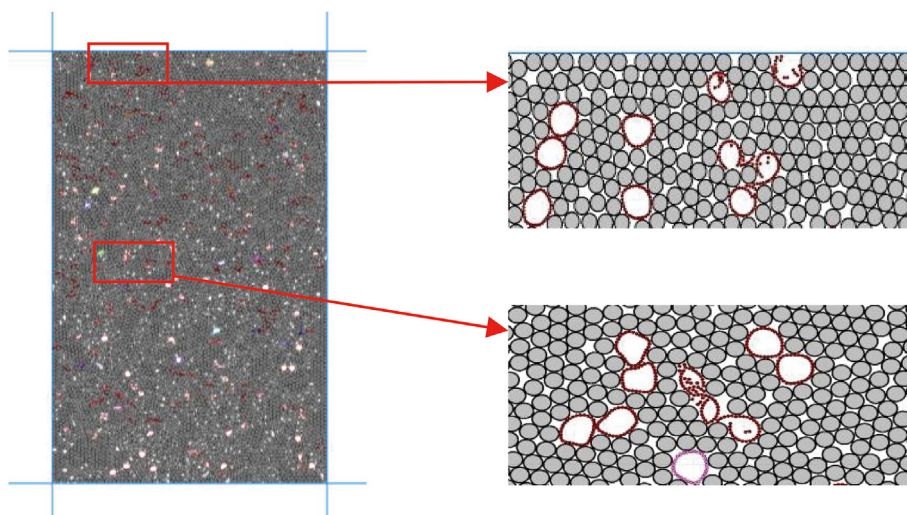


Fig. 4. Geometry of hollow microbeads in cement sheath under confining pressure.

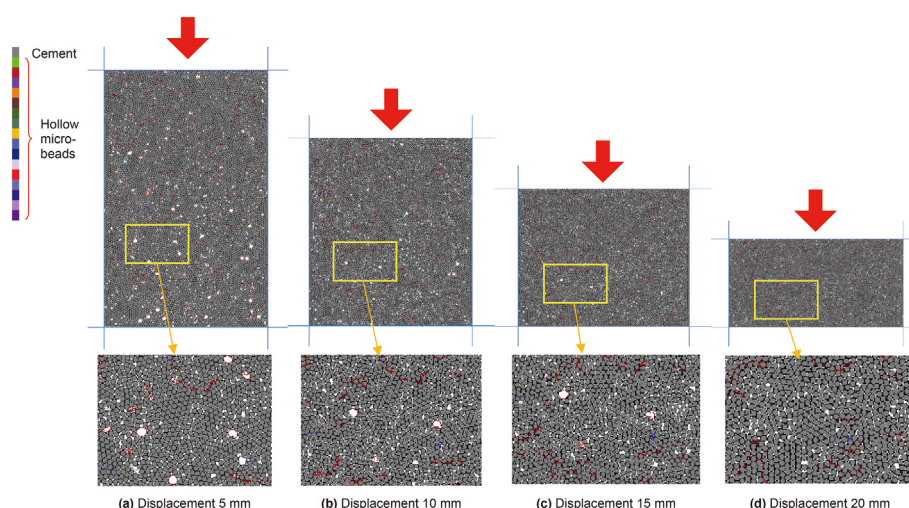


Fig. 5. Compression process of high-strength hollow microbeads in cement sheath.

formation slip is 20 mm, and the cement shows the characteristics of axial compression and transverse extension due to the limit of constant confining pressure boundary.

Fig. 6 shows the displacement distribution in cement with different hollow beads contents after formation slip. As can be seen from Fig. 6, the radial displacement becomes more uniform with higher particle content. This means the displacement transposition effect is better. Fig. 7 shows the adhesion distribution of compressed particles with the slippage of 20 mm. There are mainly two forms in cement: block and dispersion. As can be seen from Fig. 7, The gray zone is in the uncemented state between particles, which accounts for about 60%. The cemented particles (blue zone) are evenly dispersed in the cement, the supporting and protecting performance of cement is weakened.

3. Extrusion test of casing-cement system

3.1. Experimental device

The device for casing deformation simulation in Fig. 8 is mainly composed of host frame, mechanical loading system, temperature

control system, strain measurement system, data acquisition system. It can realize the axial tension/compression, shear, external extrusion under different temperature (Yang et al., 2023). A simulated wellbore was prepared before extrusion. The steel grade of casing is 110 ICY, 125 SG and 140 V, the outer diameter is 139.7 and 128.1 mm, the thickness is 10.54 and 9.17 mm. The cement thickness is 38.1 mm. The water/cement ratio is 0.44. The mixed cement slurry of class G was poured into the annular space between the casing and the iron ring. The curing time was 15 days under the temperature of 80 °C. The wellbore was placed on the fixture after preparation, and the extrusion force was applied to the wellbore by the loading system. The outer ring of simulated wellbore was removed to observe deformed casing and broken cement.

3.2. Experimental scheme

According to the statistical data in southwestern China, about 77% of casing was damaged by extrusion and 23% was damaged by shear. The casing deformation caused by external extrusion is the main failure mode during hydraulic fracturing. Therefore, the wellbore was extruded under non-uniform loading. The casing

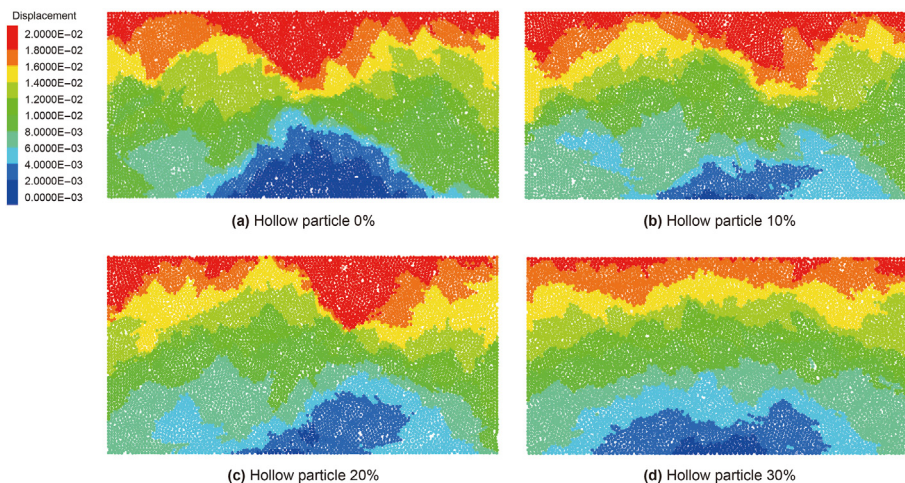


Fig. 6. Displacement distribution of cement with different contents of hollow microbeads after formation slip.

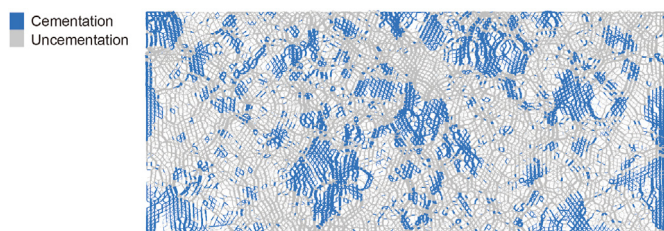


Fig. 7. Adhesion distribution of compressed particles.

length was 0.8 m, and the clamps were squeezed 20 mm respectively in experiment. The appearance, size and deformation of the casing were measured and analyzed after extrusion. The specific experimental scheme is shown in Table 2. Among them, elastic cement slurry was used in No.1#, 6# and 11# experiment, cement slurry with 10% high strength hollow microbeads was used in No.2#, 7# and 12# experiment, and cement slurry with 20% high strength hollow microbeads was used in the other experiments. The properties of cement slurry are shown in Table 3. According to the downhole performance requirements of hollow particles, the compressive strength of hollow particle is selected as 52.7 MPa, and the density range is between 0.60 and 0.66 g/cm³. It can be seen that the deformation degree is mainly distributed in the range of 10%–20%. Deformation degree increases with the increase of casing

diameter and thickness. Deformation degree is decreased with a higher proportion of hollow microbeads. The reason is that the broken hollow microbeads absorb part of formation displacement, which greatly protects the casing string.

3.3. Numerical model

According to the non-uniform extrusion test, the casing-cement model in Fig. 9 was set up. Based on experiment 3#, the Poisson's ratio of casing is 0.24, its elastic modulus is 213 GPa, and its yield strength is 836 MPa. The two clamps were squeezed 20 mm respectively in the numerical model. The shape, deformation and stress variation of the casing during extrusion were observed.

Fig. 10 shows the casing deformation degree and stress distribution after extrusion. It can be seen from Fig. 10 that the casing is reduced due to non-uniform extrusion. The calculation show that the minimum diameter after extrusion is 117.8 mm, and the minimum diameter measured after experiment is 118.3 mm. The error is only 2.3%. Compared with the morphology of the extruded cement in Fig. 11, the wellbore is obviously compressed at the extruded position, especially the cement sheath. The thickness of the extruded area is significantly reduced with comminution failure of cement sheath. The shape of cement sheath after extrusion is shown in Fig. 11. There are local cracks in cement under the extrusion force. According to the above numerical and experimental results, the numerical model can effectively trace the

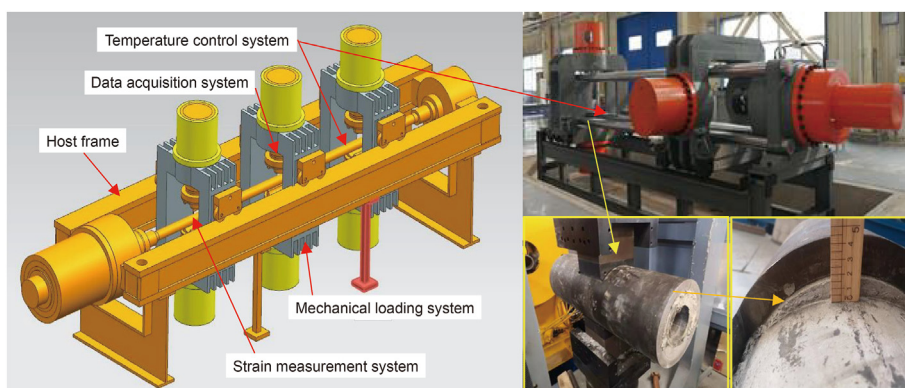


Fig. 8. The experimental device.

Table 2
Thickness and outer diameter of casing-cement sheath with different specifications in experiment.

No	Steel grade, ksi	Thickness, mm	Outer diameter, mm	Inner diameter, mm	Hollow particle content, %	Minimum inner diameter after extrusion of 40 mm, mm	Value of deformation, mm	Degree of deformation, %
1	110	10.54	139.7	118.62	0	96.55668	22.06332	18.6
2	110	10.54	139.7	118.62	10	98.33598	20.28402	17.1
3	110	10.54	139.7	118.62	20	100.47114	18.14886	15.3
4	110	9.17	139.7	121.36	20	100.97152	20.38848	16.8
5	110	10.59	128.1	106.92	20	95.05188	11.86812	11.1
6	125	10.54	139.7	118.62	0	97.98012	20.63988	17.4
7	125	10.54	139.7	118.62	10	100.58976	18.03024	15.2
8	125	10.54	139.7	118.62	20	103.08078	15.53922	13.1
9	125	9.17	139.7	121.36	20	103.64144	17.71856	14.6
10	125	10.59	128.1	106.92	20	97.19028	9.72972	9.1
11	140	10.54	139.7	118.62	0	100.47114	18.14886	15.3
12	140	10.54	139.7	118.62	10	103.7925	14.8275	12.5
13	140	10.54	139.7	118.62	20	106.04628	12.57372	10.6
14	140	9.17	139.7	121.36	20	106.91816	14.44184	11.9
15	140	10.59	128.1	106.92	20	98.79408	8.12592	7.6

Table 3
Parameters of cement slurry.

Slurry type	Temperature, °C	Density, g/cm ³	Initial consistency, Bc	Thickening time, min	Compressive strength in 48 h, MPa
Ordinary cement	100	1.83	23	150	23.4
Cement with 10% particle	100	1.81	24	162	20.8
Cement with 20% particle	100	1.78	28	168	19.6

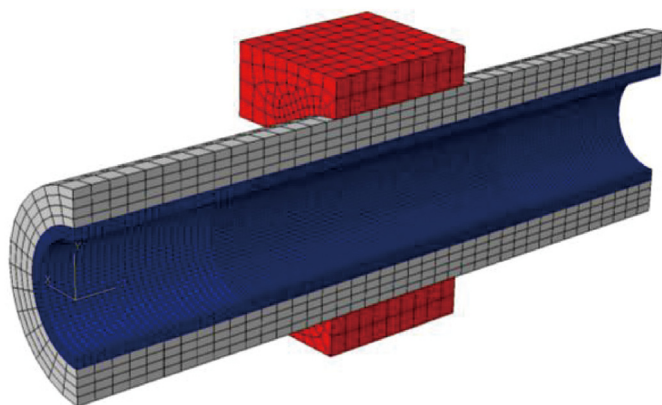


Fig. 9. Numerical model.

casing-cement extrusion process. It shows that the modified cement sheath has a certain protective effect on the casing by comparing casing deformation degree with different hollow particle content.

3.4. Analysis of influencing factors

The steel grade, casing thickness, particle size and particle content were varied in experiment to investigate the influence on casing deformation degree after slippage. Fig. 12(a) shows the relationship between casing deformation degree and formation slippage under different casing steel grade. According to Fig. 12(a), the deformation degree gradually decreases with the increase of casing steel grade. The larger formation slip, the more obvious the reduction degree. Fig. 12(b) shows the relationship between casing deformation degree and formation slippage under different casing thickness. According to Fig. 12(b), the deformation degree gradually decreases with the increase of casing thickness. The larger formation slip, the more obvious the reduction degree. However,

improving the steel grade and casing thickness will make the well construction cost rise sharply on the field.

Fig. 12(c) shows the relationship between casing deformation degree and formation slippage under different hollow particle sizes. According to Fig. 12(c), the deformation degree gradually decreases with the increase of particle size. The larger formation slip, the more obvious the reduction degree. Fig. 12(d) shows the relationship between casing deformation degree and formation slippage under different hollow particle contents. According to Fig. 12(d), the deformation degree gradually decreases with the increase of particle content. The larger the formation slip, the more obvious the reduction degree. The influence degree of the particle size and content on the casing deformation degree is larger than that of the casing steel grade and thickness. The addition of particles will not affect the drilling and fracturing process on the field, and the prevention effect of casing deformation is more obvious.

4. Field test

The geostress is heterogeneous in Weiyuan Gas Field of Sichuan Basin in China, and the casing string has been subjected to non-uniform extrusions chronically. In addition, the propagation of artificial fractures and the local pressure in the fracture will change the stress distribution near the wellbore, thus aggravating the extrusion load on the casing (Zhang et al., 2020b). The statistical analysis of casing deformation locations for 20 platforms in Block 204 of Weiyuan area shows that the casing deformation is concentrated near the inclined section at point A in Fig. 13, and the proportion of deformation decreases from point A to point B. This rule is also consistent with the engineering practice. Fracturing procedure moves gradually from point B to point A in engineering, and the deformation caused by each stage will gradually accumulate. The closer position is to point A, the larger deformation possibility will be.

In order to prove the effect of hollow particle on preventing casing deformation, wells 18-5, 38-4 and 40-3 in Block 204 of Weiyuan area were selected to use cement slurry with 15% hollow

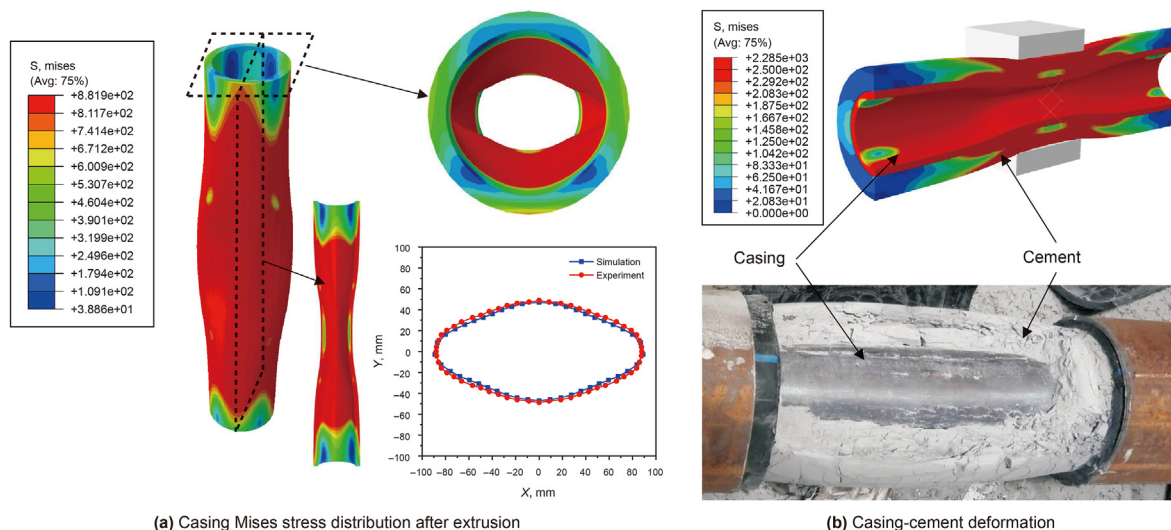


Fig. 10. Comparison between numerical and experimental results.



Fig. 11. Failure pattern of modified cement sheath after extrusion.

particle. Class G oil well cement was used in the other wells of the three platforms. The cement slurry of the offset wells is the ordinary cement system without hollow particles. The water-cement ratio is 0.44, and the its density ranges from 1.80 to 1.82 g/cm³. The hard trip of downhole tools in the test wells was compared with the surrounding offset wells. Fig. 14 shows the fault numbers encountered by 22 wells in the three platforms. The number of faults mainly distributed in 3–6. Table 4 shows the statistical results of the casing deformation in these wells in Weiyuan block. There is no downhole hard trip in W204H38–4 and W204H40–3, while the surrounding wells all have. Besides that, the W204H18–5 encountered downhole sticking three times, W204H18–4 and W204H18–6 encountered sticking five and four times respectively. The prevention effect of casing deformation in W204H18–5 cannot be judged only by the sticking times. The reason is the fault zone at Platform 18# is widely distributed and the fault is relatively active. Logging data of MIT24 arm in well W204H18–5 and W204H18–6 show that the maximum casing deformation degree in well 5 is 8.7 mm. The maximum casing deformation degree of well 6 is 11.2 mm. Therefore, the modified cement slurry system can effectively reduce the possibility of downhole hard trip in the fracturing process, and effectively control the downhole casing deformation degree.

5. Discussion

According to Section 3 and 4, the formation slip can be effectively absorbed by adding hollow particles into the cement slurry and the degree of casing deformation is reduced. The cement breaking process and the stress-strain differences of casing was briefly summarized before and after adding hollow particles in Fig. 15. As the blue line in Fig. 15, the cement steps into the elastic state firstly when the formation begins to extrude the wellbore. The cement transits into the plastic state as the displacement loading continues to increase. Because the particle is more brittle than cement, the particles start breaking once the compressive strength is reached. When the particle and cement damage to a certain extent, the combination steps into a stable plastic stage until the end of slip. Before adding the hollow particles, the radial displacement will increase sharply when the load rises to a certain value due to the poor cement compressibility, as the red line of Fig. 15. However, the load will be shared with the addition of hollow particles due to the strong compressibility and the casing radial displacement will be controlled.

6. Conclusion

The fracture mechanism of hollow particles in cement sheath was analyzed by discrete element method in this paper, and the

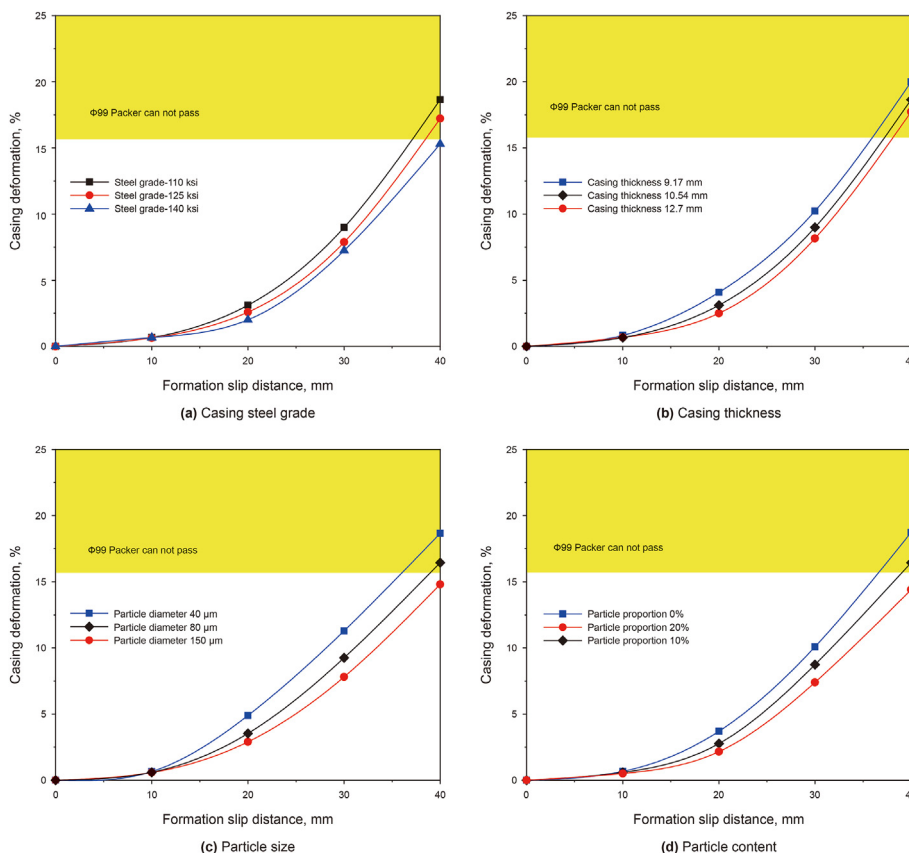


Fig. 12. Influence of different factors on casing inner diameter after formation slip.

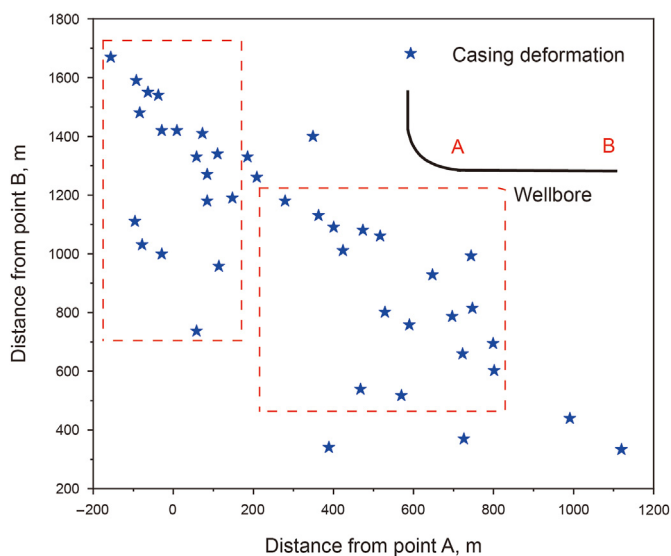


Fig. 13. Location statistics of casing deformation in Block 204 of Weiyuan Zone.

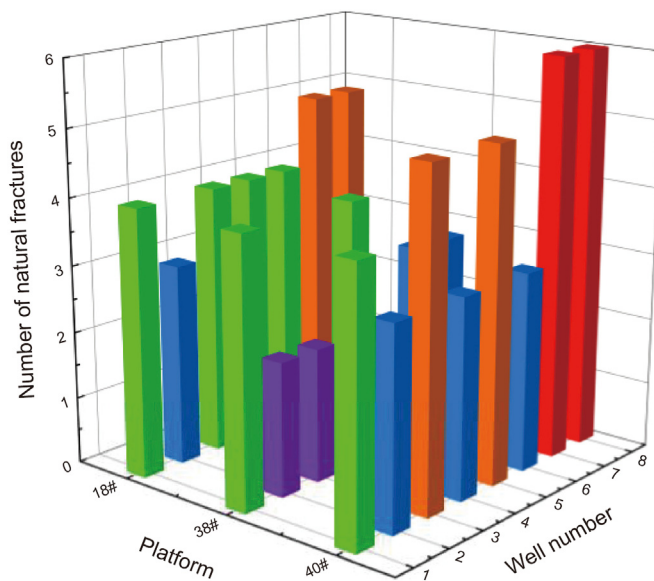


Fig. 14. Fault number encountered in each well.

influence of hollow cement on casing deformation degree was investigated by laboratory experiment. According to the experimental results and field application, the casing deformation prevention technology based on cement slurry modification was summarized, and the conclusions were as follow.

- (1) The cement sheath has good compressibility by adding hollow particles into the cement slurry when the formation slips. The particles can effectively absorb the formation displacement and transfer the excessive casing deformation.
- (2) The experimental results show that the larger the diameter and content of hollow particles, the lower the casing deformation degree after formation slip. Compared with

Table 4
Casing deformation statistics of test wells in Weiyuan block.

No	Well number	Number of designed segments	Whether to use hollow cement	Number of stages which the fracturing tool is blocked
1	W204H18-1	17	No	2
2	W204H18-2	18	No	4
3	W204H18-3	18	No	5
4	W204H18-4	18	No	5
5	W204H18-5	18	Yes	3
6	W204H18-6	18	No	4
7	W204H18-7	18	No	4
8	W204H38-1	17	No	0
9	W204H38-2	18	No	4
10	W204H38-3	17	No	15
11	W204H38-4	17	Yes	0
12	W204H38-5	17	No	6
13	W204H38-6	18	No	4
14	W204H38-7	17	No	0
15	W204H40-1	18	No	2
16	W204H40-2	18	No	0
17	W204H40-3	19	Yes	0
18	W204H40-4	18	No	2
19	W204H40-5	18	No	0
20	W204H40-6	18	No	2
21	W204H40-7	18	No	2
22	W204H40-8	18	No	2

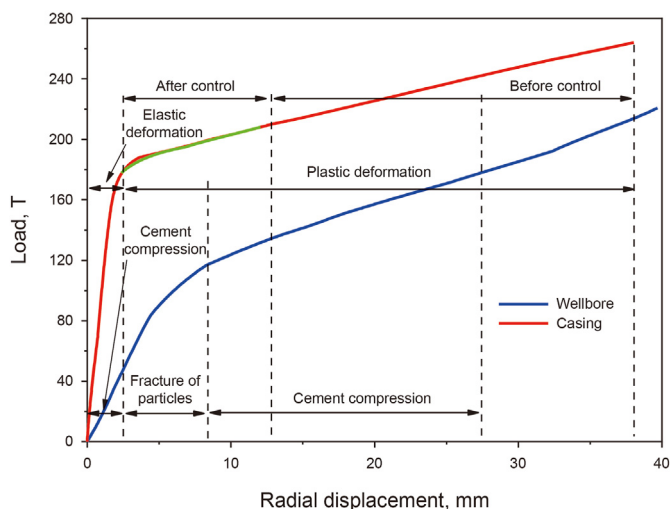


Fig. 15. Illustration of deformation prevention technology based on cement slurry modification.

improving the steel grade and thickness of casing, the parameters of hollow particles in cement have a larger influence on the degree of casing deformation mitigation.

- (3) Based on the serious casing deformation of shale gas well in southwestern China, a casing deformation control method based on modified cement slurry was set up by means of numerical simulation and laboratory test. According to the feedback of field tests, the modified cement slurry system can decrease the casing deformation degree by 11.9% when the proportion of hollow particles is 15%, ensuring the smooth trip of fracturing tools.

CRediT authorship contribution statement

Yan Yan: Conceptualization, Data curation, Formal analysis, Investigation, Methodology, Software, Writing – original draft, Writing – review & editing. **Meng Cai:** Investigation, Resources.

Wen-Hai Ma: Investigation, Resources. **Xiao-Chuan Zhang:** Investigation, Resources. **Li-Hong Han:** Supervision, Validation, Visualization, Funding acquisition. **Yong-Hong Liu:** Supervision, Visualization.

Declaration of competing interest

We confirm that there are no potential competing interests for this article.

Acknowledgements

The authors would like to gratefully acknowledge the supports of project funded by China Postdoctoral Science Foundation (2023M743886), Project of Shale Gas Evaluation and Exploitation Key Laboratory of Sichuan Province (YSK2023004), youth project funded by Shaanxi Province Natural Science Basic Research Program (2024JC-YBQN-0522).

References

- Adjei, S., Elkatatny, S., Sarmah, P., et al., 2021. Investigation of dehydroxylated sodium bentonite as a pozzolanic extender in oil-well cement. *SPE Drill. Complet.* 36 (3), 730–737. <https://doi.org/10.2118/205487-PA>.
- Cheng, Y.Q., Liu, S.Q., Shen, J.Y., et al., 2023. Matching analysis and experimental study of mechanical properties of cement sheath interface. *J. Petrol. Sci. Eng.* 220, 111138. <https://doi.org/10.1016/j.petrol.2022.111138>.
- Dong, K., Liu, N.Z., Chen, Z.W., et al., 2019. Geomechanical analysis on casing deformation in Longmaxi shale formation. *J. Petrol. Sci. Eng.* 177, 724–733. <https://doi.org/10.1016/j.petrol.2022.111138>.
- Furui, K., Fuh, G., Morita, N., et al., 2012. Casing-and screen-failure analysis in highly compacting sandstone fields. *SPE Drill. Complet.* 27 (2), 241–252. <https://doi.org/10.2118/146231-PA>.
- Guo, S.L., Bu, Y.H., Zhou, A.N., et al., 2020. A three components thixotropic agent to enhance the thixotropic property of natural gas well cement at high temperatures. *J. Nat. Gas Sci. Eng.* 84, 103699. <https://doi.org/10.1016/j.jngse.2020.103699>.
- Guo, X.L., Li, J., Liu, G.H., et al., 2019. Numerical simulation of casing deformation during volume fracturing of horizontal shale gas wells. *J. Petrol. Sci. Eng.* 172, 731–742. <https://doi.org/10.1016/j.petrol.2018.08.067>.
- Hudson, M.D., Sheperd, P., Ricci, J., 2017. Flexible cement slurry survives multistage hydraulic fracturing treatment. In: *SPE Unconventional Resources Conference*. February 15–16, Alberta, Canada. <https://doi.org/10.2118/185068-MS>.
- Jafariefad, N., Geiker, M.R., Skalle, P., 2017a. Nanosized magnesium oxide with engineered expansive property for enhanced cement-system performance. *SPE J.* 22 (5), 1681–1689. <https://doi.org/10.2118/180038-PA>.
- Jafariefad, N., Sangesland, S., Gawel, K., et al., 2020. New materials and

- technologies for life-lasting cement sheath: a review of recent advances. *SPE Drill. Complet.* 35 (2), 262–278. <https://doi.org/10.2118/199885-PA>.
- Jafariefad, N., Geiker, M.R., Gong, Y., et al., 2017b. Cement sheath modification using nanomaterials for long-term zonal isolation of oil wells: Review. *J. Petrol. Sci. Eng.* 156, 662–672. <https://doi.org/10.1016/j.petrol.2017.06.047>.
- Li, H.T., Li, Z., Li, G., et al., 2020. Casing deformation mechanisms of horizontal wells in Weirong shale gas field during multistage hydraulic fracturing. *J. Nat. Gas Sci. Eng.* 84, 103646. <https://doi.org/10.1016/j.jngse.2020.103646>.
- Li, H., Yang, C.H., Ma, H.L., et al., 2020. A 3D grain-based creep model (3D-GBCM) for simulating long-term mechanical characteristic of rock salt. *J. Petrol. Sci. Eng.* 185, 106672. <https://doi.org/10.1016/j.petrol.2019.106672>.
- Li, Z., Li, G., Li, H., et al., 2021a. A novel investigation on casing deformation during hydraulic fracturing in the Weirong shale gas field, Sichuan basin, China. *Arabian J. Geosci.* 14 (24), 1–15. <https://doi.org/10.1007/s12517-021-09040-9>.
- Li, Z., Li, H., Li, G., et al., 2021b. The influence of shale swelling on casing deformation during hydraulic fracturing. *J. Petrol. Sci. Eng.* 205 (9), 108844. <https://doi.org/10.1016/j.petrol.2021.108844>.
- Lian, Z.H., Yu, H., Lin, T.J., et al., 2015. A study on casing deformation failure during multi-stage hydraulic fracturing for the stimulated reservoir volume of horizontal shale wells. *J. Nat. Gas Sci. Eng.* 23, 538–546. <https://doi.org/10.1016/j.jngse.2015.02.028>.
- Liu, K., Gao, D.L., Yang, J., et al., 2019a. Effect of expandable cement on increasing sealing ability of cement sheath in shale gas wells. *J. Petrol. Sci. Eng.* 176, 850–861. <https://doi.org/10.1016/j.petrol.2019.01.077>.
- Liu, K., Taleghani, A.D., Gao, D.L., 2019b. Calculation of hydraulic fracture induced stress and corresponding fault slippage in shale formation. *Fuel* 254, 115525. <https://doi.org/10.1016/j.fuel.2019.05.108>.
- Meng, H., Ge, H.K., Fu, D.W., et al., 2020. Numerical investigation of casing shear deformation due to fracture/fault slip during hydraulic fracturing. *Energy Sci. Eng.* 8 (10), 1–14. <https://doi.org/10.1002/ese3.766>.
- Peng, S.P., Fu, J.T., Zhang, J.C., 2007. Borehole casing failure analysis in unconsolidated formations: a case study. *J. Petrol. Sci. Eng.* 59 (4), 226–238. <https://doi.org/10.1016/j.petrol.2007.04.010>.
- Quercia, G., Brouwers, H.J.H., Garnier, A., et al., 2016. Influence of olivine nano-silica on hydration and performance of oil-well cement slurries. *Mater. Des.* 96, 162–170. <https://doi.org/10.1016/j.matdes.2016.02.001>.
- Salehi, S., Khattak, M.J., Ali, N., et al., 2018. Study and use of geopolymer mixtures for oil and gas well cementing applications. *J. Energy Resour. Technol.* 140 (1), 012908. <https://doi.org/10.1115/1.4037713>.
- Santos, L., Taleghani, A.D., Li, G., 2021. Nanosilica-treated shape memory polymer fibers to strengthen wellbore cement. *J. Petrol. Sci. Eng.* 196, 107646. <https://doi.org/10.1016/j.petrol.2020.107646>.
- Teodoriu, C., Yi, M.C., Salehi, S., 2019. A Novel experimental investigation of cement mechanical properties with application to geothermal wells. *Energies* 12 (18), 3426. <https://doi.org/10.3390/en12183426>.
- Wang, Y.B., Liu, K., Gao, D.L., 2021. Investigation of the interface cracks on the cement sheath stress in shale gas wells during hydraulic fracturing. *J. Petrol. Sci. Eng.* 205, 108981. <https://doi.org/10.1016/j.petrol.2021.108981>.
- Wei, S.M., Kuru, E., Jin, Y., et al., 2022. Numerical investigation of the factors affecting the cement sheath integrity in hydraulically fractured wells. *J. Petrol. Sci. Eng.* 215, 110582. <https://doi.org/10.1016/j.petrol.2022.110582>.
- Xi, Y., Jiang, J.W., Li, J., et al., 2021. Research on the influence of strike-slip fault slippage on production casing and control methods and engineering application during multistage fracturing in deep shale gas wells. *Energy Rep.* 7, 2989–2998. <https://doi.org/10.1016/j.egy.2021.05.039>.
- Xi, Y., Li, J., Fan, L.F., et al., 2020. Mechanism and numerical simulation of a new device of bypass cementing device for controlling casing shear deformation induced by fault slippage. *J. Petrol. Sci. Eng.* 196 (5), 107820. <https://doi.org/10.1016/j.petrol.2020.107820>.
- Xi, Y., Li, J., Liu, G.H., et al., 2019. A new numerical method for evaluating the variation of casing inner diameter after strike-slip fault sliding during multistage fracturing in shale gas wells. *Energy Sci. Eng.* 7, 2046–2058. <https://doi.org/10.1002/ese3.410>.
- Xi, Y., Li, J., Liu, G.H., et al., 2018. Numerical investigation for different casing deformation reasons in Weiyuan-Changning shale gas field during multistage hydraulic fracturing. *J. Pet. Sci. Eng.* 163, 691–702. <https://doi.org/10.1016/j.petrol.2017.11.020>.
- Yan, W., Zou, L.Z., Li, H., et al., 2017. Investigation of casing deformation during hydraulic fracturing in high geo-stress shale gas play. *J. Pet. Sci. Eng.* 150, 22–29. <https://doi.org/10.1016/j.petrol.2016.11.007>.
- Yang, S.Y., Zeng, B., Yan, Y., et al., 2023. Research on casing deformation mechanism and prevention technology in salt rock creep formation. *J. Petrol. Sci. Eng.* 220, 111176. <https://doi.org/10.1016/j.petrol.2022.111176>.
- Yin, F., Han, L.H., Yang, S.Y., et al., 2018a. Casing deformation from fracture slip in hydraulic fracturing. *J. Petrol. Sci. Eng.* 166, 235–241. <https://doi.org/10.1016/j.petrol.2018.03.010>.
- Yin, F., Xiao, Y., Han, L.H., et al., 2018b. Quantifying the induced fracture slip and casing deformation in hydraulically fracturing shale gas wells. *J. Nat. Gas Sci. Eng.* 60, 103–111. <https://doi.org/10.1016/j.jngse.2018.10.005>.
- Yu, H., Taleghani, A.D., Lian, Z.H., et al., 2022. Severe casing failure in multistage hydraulic fracturing using dual-scale modeling approach. *SPE Drill. Complet.* 37 (3), 252–266. <https://doi.org/10.2118/206216-PA>.
- Yu, H., Lian, Z.H., Lin, T.J., et al., 2016. Study on failure mechanism of casing in stimulated reservoir volume fracturing of shale gas. *J. Safety Sci. Tech.* 12 (10), 37–43. <https://doi.org/10.11731/j.issn.1673-193x.2016.10.006>.
- Zhang, F.S., Yin, Z.R., Chen, Z.W., et al., 2020a. Fault reactivation and induced seismicity during multistage hydraulic fracturing: microseismic analysis and geo-mechanical modeling. *SPE J.* 25 (2), 692–711. <https://doi.org/10.2118/199883-PA>.
- Zhang, F.S., Jiang, Z.Y., Chen, Z.W., et al., 2020b. Hydraulic fracturing induced fault slip and casing shear in Sichuan Basin: a multi-scale numerical investigation. *J. Petrol. Sci. Eng.* 195, 107797. <https://doi.org/10.1016/j.petrol.2020.107797>.
- Zhao, C.J., Li, J., Zaman, M., et al., 2021. Investigation of casing deformation characteristics under cycling loads and the effect on casing strength based on full-scale equipment. *J. Petrol. Sci. Eng.* 205, 108973. <https://doi.org/10.1016/j.petrol.2021.108973>.